

When and why the Neo-Tethyan subduction initiated along the Eurasian margin: a case study from a Jurassic eclogite in southern Iran

Bo Wan¹, Yang Chu², Ling Chen², Zhiyong Zhang², Songjian Ao², and Morteza Talebian³

¹Chu State Key Laboratory of Lithospheric Evolution, Institute of Geology and Geophysics, Chinese Academy of Sciences, Beijing 100029, China

²State Key Laboratory of Lithospheric Evolution, Institute of Geology and Geophysics, Chinese Academy of Sciences, Beijing 100029, China

³b Research Institute for Earth Sciences, Geological Survey of Iran

January 20, 2023

Abstract

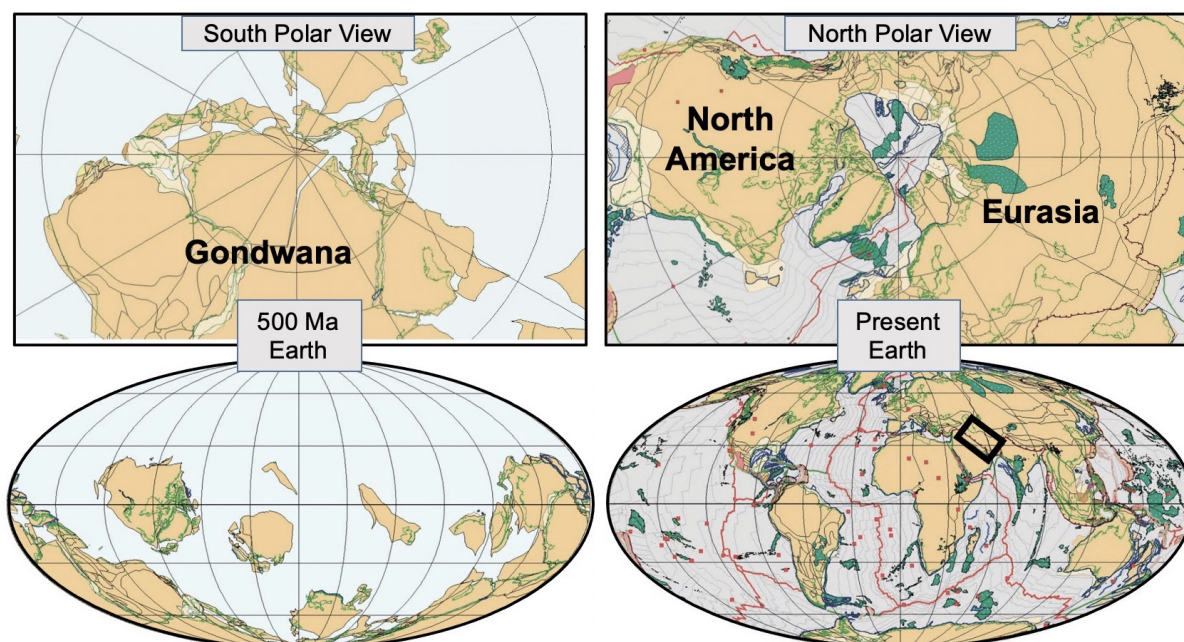
Tethyan evolution is characterized by cyclical continent-transfer from Gondwana to the continents in the Northern Hemisphere, similar to a “one-way” train. Subduction has been viewed as the primary driver of transference. Therefore, it is crucial to understand the tectonic evolution of all past subduction zones that occurred along Eurasia’s southern margin. We studied the earliest known eclogite located at the Neo-Tethyan suture in the Iranian segment. A prograde-E-MORB-like eclogite reached a peak metamorphic condition of 2.2 GPa and 560°C, at 190 ± 11 Ma (1? rutile U-Pb ages), which constrains the youngest age for subduction initiation of the Neo-Tethyan slab. Combined with regional magmatic and structural data, the oldest age for Neo-Tethys subduction initiation is 210–192 Ma, which is younger than the Paleo-Tethyan closure time of 228–209 Ma. These data, used with previous numerical modeling, supports collision-induced subduction initiation. The collision-induced force, together with the Paleo-Tethyan subduction driven-mantle flow, is likely to have exploited weak inherited structures from earlier Neo-Tethyan rifting, resulting in a northward directed subduction zone along the southern margin of Central Iran Block.

24 Abstract

25 Tethyan evolution is characterized by cyclical continent-transfer from Gondwana to
26 the continents in the Northern Hemisphere, similar to a “one-way” train. Subduction
27 has been viewed as the primary driver of transference. Therefore, it is crucial to
28 understand the tectonic evolution of all **past** subduction zones that occurred along
29 Eurasia's southern margin. We studied the earliest known eclogite located at the
30 Neo-Tethyan suture in the Iranian segment. A prograde-E-MORB-like eclogite
31 reached a peak metamorphic condition of 2.2 GPa and 560°C, at 190 ± 11 Ma (**1 σ**
32 rutile U-Pb ages), which constrains the youngest age for subduction initiation of the
33 Neo-Tethyan slab. Combined with regional magmatic and structural data, the oldest
34 age for Neo-Tethys subduction initiation is 210–192 Ma, which is younger than the
35 Paleo-Tethyan closure time of 228–209 Ma. These data, used with previous
36 numerical **modeling**, supports collision-induced subduction initiation. The collision-
37 induced force, together with the Paleo-Tethyan subduction driven-mantle flow, is
38 likely to have exploited weak inherited structures from earlier Neo-Tethyan rifting,
39 resulting in a northward directed subduction zone along the southern margin of
40 Central Iran **Block**.

41 **Key words:** continental rifting, collision-induced, subduction initiation, Neo-Tethyan,
42 Tethyan dynamics

43



45
 46 **Figure 1. Views of Earth. Left: the South Polar view of the Earth and world map**
 47 **(at 500 Ma); Right: the North Polar map of the Earth and world map (present**
 48 **day) adapted from Lawver et al. (2015). Light grey: continent; dark grey: large**
 49 **igneous provinces. The study area is denoted by a black square.**

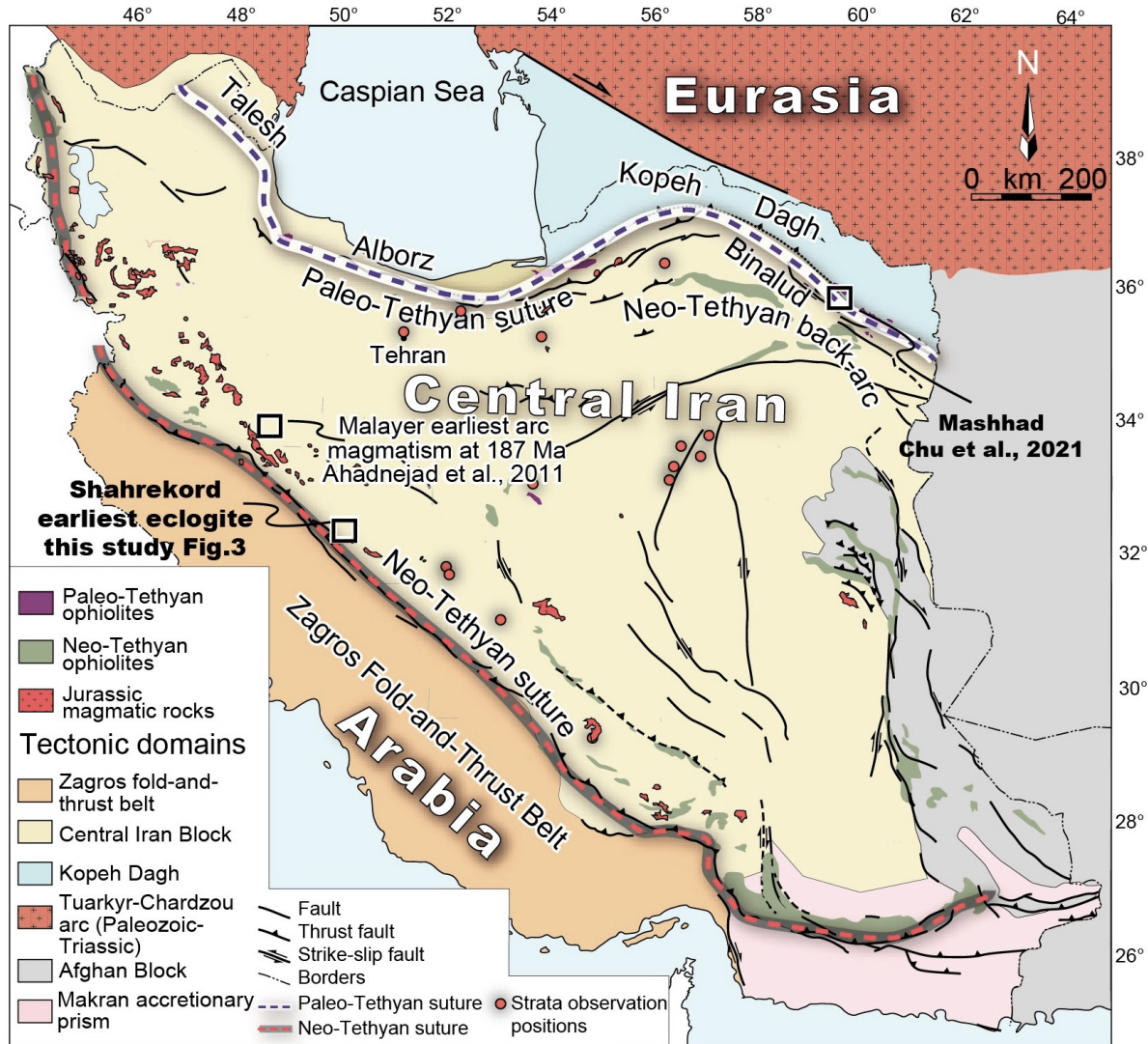
50
 51 Currently, with the exception of Antarctica, most continents are connected and
 52 encircle the north pole (Fig. 1). Almost all continents, including Gondwana, were
 53 located in the central to southern hemisphere to cap the south pole at about 500 Ma
 54 (Lawver et al., 2015). The one-way mega-transferring of continents from south to
 55 north was a key event of Earth, that occurred during the last 500 million years (Myr),
 56 with the Australian continent moving north at a rate of 70 mm/year as a
 57 representative active example (DeMets et al., 2010). During this mega-transferring of
 58 continents, the sea-land paleogeography changed, which influenced the Earth's
 59 surface temperature from an icy to a warmer world (Merdith et al., 2019; Bergman et
 60 al., 2021; Scotese et al., 2021). However, the driving mechanism for this one-

61 way/single-directed transfer is still debated. Two competing theories are: (1) whole
62 mantle convection which involves plume upwelling and subduction (e.g. Becker and
63 Faccenna, 2011; Jolivet et al., 2016; Faccenna et al., 2021); and (2) northward
64 oceanic subduction (Wan et al., 2019; Wu et al., 2020). After 50 Ma, the Indo-
65 Australian oceanic plate began subducting beneath the southern Eurasian continent
66 (Sunda Shelf) margin along the Java trench (Hall, 2017). The major eruption of the
67 Kerguelen large igneous province (90–120 Ma) has been proposed to have
68 fragmented the Antarctic-Australia plate. However, this eruption was earlier than the
69 abrupt velocity change of the Australia plate at 45 Ma (Whittaker et al., 2013;
70 Williams et al., 2019). Instead, the Australian plate acceleration is temporally closer
71 with that of the 50 Ma Java trench subduction zone activity. This supports the idea
72 that subduction is the driving force of the northward migration of the Australian plate
73 (Forsyth and Uyeda, 1975).

74 The cycle of Tethyan oceans involved the Proto-Tethys (440–420 Ma closure),
75 the Paleo-Tethys (330–220 Ma closure), and the Neo-Tethys (65–15 Ma closure).
76 This cycle merged many Gondwana-derived continents with continents to the north.
77 All surviving Tethyan sutures are presently located in the northern hemisphere
78 (Stampfli et al., 2013; Torsvik and Cocks, 2017; Wu et al., 2020). It is unclear if the
79 closure of the Tethyan oceans was caused by the same tectonic forces that are
80 controlling the current evolution of the Indian Ocean and the northward migration of
81 the Australian plate. To compare these two scenarios, it is necessary to first
82 constrain the subduction initiation for the Tethyan oceans, in particular the youngest

83 Neo-Tethyan ocean. However, subduction initiation is a challenging and poorly
84 understood topic (Stern and Gerya, 2018), especially given the discrepancy between
85 numerical modeling (Gerya et al., 2015; Leng and Gurnis, 2015; Zhong and Li, 2020;
86 Zhou et al., 2020; Zhong and Li, 2022), and geological observations (Whattam and
87 Stern, 2011; Guilmette et al., 2018; van Hinsbergen et al., 2021).

88 The Neo-Tethyan Iranian segment preserves many Neo-Tethyan ophiolites
89 (Moghadam and Stern, 2015; Ao et al., 2016), subduction-related magmatic
90 episodes (Omrani et al., 2008; Chiu et al., 2013; Chiu et al., 2017; Zhang et al.,
91 2018; Moghadam et al., 2022), and metamorphic events (Agard et al., 2011;
92 Davoudian et al., 2016; Bonnet et al., 2020). This makes the Iranian segment an
93 ideal location to study the Neo-Tethyan subduction initiation problem. There is a
94 consensus about Neo-Tethyan subduction initiation along the southern Iranian
95 continent's margin (Hassanzadeh and Wernicke, 2016; Stern et al., 2021). However,
96 the timing of Neo-Tethyan subduction initiation in Iran is debated, and either
97 occurred in the Triassic-Jurassic (Arvin et al., 2007), or the Cretaceous (Moghadam
98 and Stern, 2015). In addition, the driving mechanism has been explained through
99 either collision-induced (Wan et al., 2019), or spontaneous nucleation (Moghadam
100 and Stern, 2011) Additionally, it is crucial to understand why the subduction of the
101 Indian, Neo-Tethyan, and Paleo-Tethyan ocean basins consistently initiate along the
102 southern Eurasian margin with a north-dipping slab, as opposed to how subduction
103 polarity frequently reverses in the southern hemisphere in the Pacific realm (Brown
104 and Ryan, 2011).



105

106 **Figure 2: Tectonic sketch map of Iran, highlighting tectonic domains, Neo-**
 107 **Tethyan suture, Jurassic magmatism, and high-pressure metamorphism.**
 108 **Based on the map from the Geological-Survey-of-Iran (2009). Strata**
 109 **observation positions from Leven and Gorgij, (2011).**

110

111

112

113

114

115

In this study, an eclogite sample along the Neo-Tethyan suture zone in southern Iran was analyzed to find out its protolith nature, in situ metamorphic age, and its corresponding metamorphic condition based on geochemical-petrological studies. The new in-situ U-Pb rutile age is the earliest subduction-related high-pressure metamorphic event observed in the Neo-Tethyan suture zone. This event defines the latest (youngest) timing of subduction initiation. In addition, the mechanism for how

116 and why subduction occurred is discussed with the goal to better understand other
117 Tethyan regions and subduction zones globally.

118

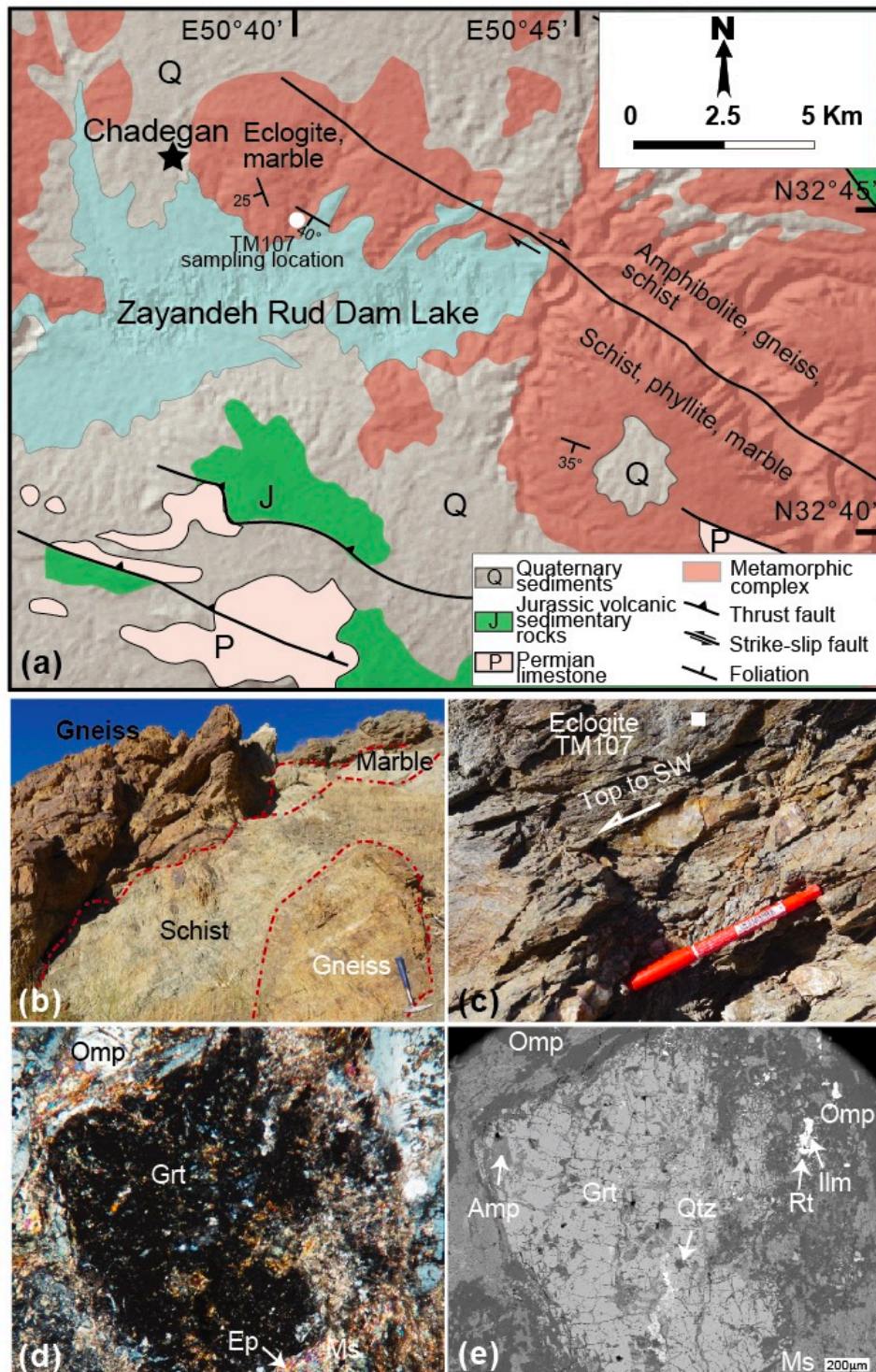
119 2. Geological background

120 Three major tectonic domains dominate the Tethyan evolution in Iran. Along the
121 Talesh-Alborz-Binalud mountain range in northern Iran, the Paleo-Tethyan suture
122 divides the Kopeh-Dagh domain to the north from the Central Iran domain to the
123 south. The Neo-Tethyan closure sutured the Central Iran domain and Arabia domain
124 in southern Iran. The Kopeh-Dagh is dominated by Jurassic to Cenozoic shallow
125 marine to continental sedimentary rocks such as: limestone, sandstone, shale, and
126 conglomerate. The basement of the Kopeh-Dagh domain is a Paleozoic–Early
127 Mesozoic volcanic arc located on the Baltic or Siberian Precambrian continents
128 (Natal'in and Şengör, 2005; Zanchetta et al., 2013; Chu et al., 2021).

129 According to sedimentary records, the entire central Iran domain was formerly
130 part of the Arabian continent but separated as a ribbon continent (Cimmeria) in the
131 late Permian (Koop et al., 1982). During the rifting and drifting process, Central Iran
132 was surrounded by passive margins, as indicated by sedimentary facies analyses
133 (Leven and Gorgij, 2011), which share a similar scenario of Indian drifting northward
134 during the Cretaceous. Recent research in northern Iran, along the Paleo-Tethyan
135 suture near Mashhad, indicate that the first arrival of Eurasian material to the passive
136 margin of central Iran occurred at 209–228 Ma (Chu et al., 2021). Previous
137 stratigraphic studies suggest that the collision must have occurred between the late

138 Triassic (228 Ma) and the mid Jurassic (174 Ma), and possibly initiated at the
139 Carnian–Norian boundary (Fürsich et al., 2009). Additionally, the extensive time
140 span might be restricted by a stitching pluton at 217 ± 1.7 Ma (2σ) that crosscuts
141 through Triassic compressional structures in the Alborz (Zanchetta et al., 2013).
142 Thus, the new detrital zircon results (209–228 Ma) (Chu et al., 2021), corroborate
143 prior stratigraphic and structural geological studies (217–228 Ma), implying a Triassic
144 collision event.

145 Magmatism is extensive in Central Iran, with two magmatic flare-ups occurring in
146 the Jurassic along southern Iran (Fig. 2), and in the Cenozoic throughout Central
147 Iran (Verdel et al., 2011; Chiu et al., 2013; Zhang et al., 2018; Moghadam et al.,
148 2022). The Jurassic plutons are mostly granite, granodiorite, quartz diorite, and
149 gabbro (Hassanzadeh and Wernicke, 2016), whilst the Jurassic volcanic rocks are
150 mostly basaltic, andesitic lava, and volcanoclastics (Emami and Khalili, 2008).
151 Geochemical studies on the Jurassic igneous rocks found $\epsilon\text{Hf}_{(T)}$ values ranging from
152 +13 to -3 (Chiu et al., 2017; Zhang et al., 2018), indicating that they originated from
153 a mixed juvenile and reworked crustal sources. The Hf isotopic ratios of Jurassic
154 igneous rocks are in the range of Cenozoic igneous rocks $\epsilon\text{Hf}_{(T)}$ (+14 to -7) along
155 southern Iran (Chiu et al., 2017; Moghadam et al., 2022). The similar petrological
156 and geochemical features between Jurassic and Cenozoic magmatic rocks implies a
157 similar subduction-related tectonic environment, while some researchers think that
158 the Jurassic rocks have inherited the geochemical signature from a Mesozoic
159 continental rifting episode (Azizi and Stern, 2019).



160

161 **Figure 3. (a) Simplified geological map showing the juxtaposition of various**
 162 **rock types and metamorphic grades of rocks, based on the Shahrekord Sheet**
 163 **of the Geological-Survey-of-Iran (2009). (b) Marble lenses in schist and gneiss.**
 164 **(c) Top-to-the-SW fabric in eclogite (white square marks the thin section site).**
 165 **Two thin section photos (d: cross polarized light, e: backscattered electron)**

166 **showing the major mineral associations. Grt: garnet, Omp: omphacite, Rt:**
167 **rutile, Amp: amphibole, Qtz: quartz, Ilm: ilimnite, ep: epidote, and Ms: mica**

168 Along southern Iran, Jurassic high-pressure low-temperature (HP/LT)
169 metamorphic rocks have been reported (Davoudian et al., 2016; Jamali Ashtiani et
170 al., 2020). The HP/LT rock is an eclogite with a peak metamorphic condition of 2.35–
171 2.5 GPa and 520–600°C, and metamorphic ages of 172–184 Ma by Ar-Ar dating of
172 phengite (Davoudian et al., 2016). The eclogites outcrop along a regional NW-
173 striking shear zone (Fig. 3), and the field relationship has been described in detail by
174 (Davoudian et al., 2016). Eclogite bodies and marbles occur as lenses in the schist,
175 and the lenses are mostly meters-scale. The marble lenses contain dark eclogite,
176 indicating the marble has also undergone HP metamorphism. The schist is at
177 amphibolite-grade, with greenschist in the surrounding region. The ages of the
178 schists are still unknown. Recent studies show that the gneisses are from Cadomian
179 basement, with an age of 552 Ma, which also containing a younger intrusion dated
180 as 176 ± 3.3 Ma (2σ) (Jamali Ashtiani et al., 2020). Permian limestone, Jurassic
181 volcanic-sedimentary rocks are thrust over the metamorphic complex with various
182 grades of metamorphic rocks such as schist, gneiss, and amphibolite. The Jurassic
183 volcanic-sedimentary rocks have experienced low-grade metamorphism, at
184 prehnite–pumpellyite facies. This type of rock assemblage, with different origin with
185 contrasting metamorphic grades is very similar to the accretionary complex
186 associated with subduction zones observed globally (Wakabayashi, 2011).

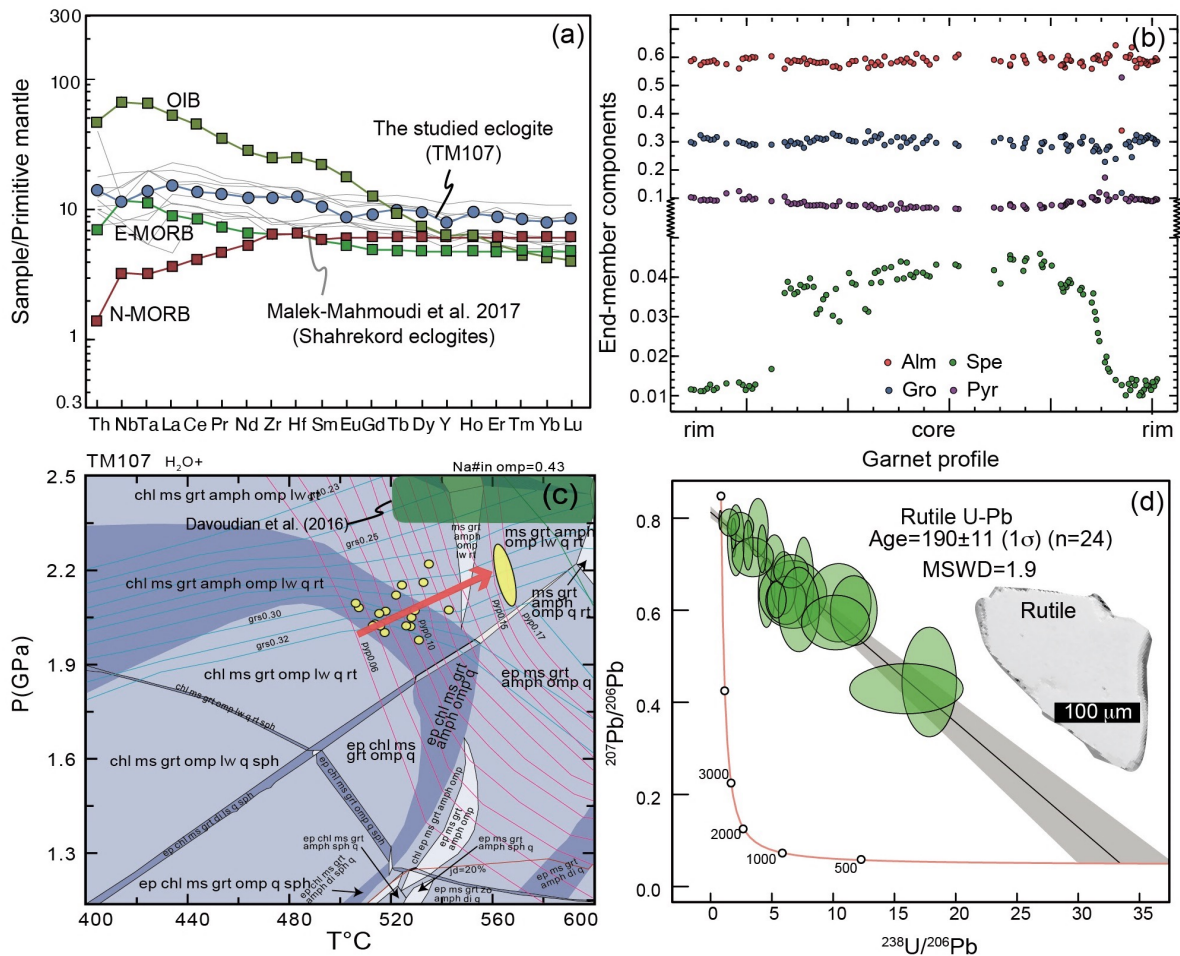
187 Additionally, understanding the origin of the HP/LT rocks will aid in comprehending
188 the subduction environment at the time.

189 Many early Cretaceous ophiolites occur in the south of Central Iran (Moghadam
190 and Stern, 2011; Moghadam and Stern, 2015), and extensive Cretaceous to
191 Cenozoic magmatic rocks are viewed as the subduction products of the Neo-
192 Tethyan slab (Omrani et al., 2008; Moghadam et al., 2022). The final closure of the
193 Neo-Tethys merged the Central Iran domain with the Zagros domain along the
194 Zagros suture during the Oligocene or the Miocene (McQuarrie and van Hinsbergen,
195 2013; Zhang et al., 2017).

196

197 3. Sample, analytical methods and results

198 In the Shahrekord region, we sampled an eclogite (TM107, N32°45'47"
199 E50°39'37") near Chadegan (Fig. 3). The eclogite is composed of garnet, omphacite,
200 muscovite, chlorite, barroisite, calcic-amphibole, epidote, quartz, rutile, and ilmenite.
201 The metamorphic mineral assemblage at its peak is composed of amphibole,
202 muscovite, garnet, omphacite, quartz, and rutile.



203

204 **Figure 4. Analytical results from bulk sample or minerals from studied eclogite**
 205 **sample TM107. (a) Primitive mantle-normalized trace-element pattern,**
 206 **normalizing data from Sun and McDonough (1989). (b) EMPA profiles**
 207 **showing homogenous components of Mg, Ca, Al and decreasing Mn**
 208 **garnet end-member components from core to rim in garnet grain; (c). P–T**
 209 **pseudosection (SiO₂ 48.23, TiO₂ 1.89, Al₂O₃ 14.51, FeO 12.86, MgO 7.54,**
 210 **CaO 11.18, Na₂O 2.62, MnO 0.24, K₂O 0.65 wt.%, which is corrected from**
 211 **table 1). Ellipse region is calculated from EPMA data of garnet**
 212 **(Supplementary table), and rectangle region from Davoudian et al. (2016).**
 213 **(d) Rutile SIMS U-Pb age.**

214

215

216

The sample was ground the sample into 200-mesh powder and the bulk-sample's major and trace elements geochemistry was analyzed to determine the rock's origin. To understand the metamorphic processes and peak metamorphic

217 conditions, we chose a representative garnet was selected for major oxide
218 measurements and P-T pseudosection modeling. Additionally, rutile was separated
219 and the U-Pb isotopes were analyzed to determine the absolute age of peak
220 metamorphism. Rutile was used as it formed at a peak metamorphic stage, is in
221 equilibrium with garnet, and has an appropriate U-Pb system closure temperature of
222 ~600°C, with a proper crystal size (Cherniak, 2000). The analyses were undertaken
223 by various facilities at the Institute of Geology and Geophysics, Chinese Academy of
224 Sciences. The details are described in the supplementary file.

225 The eclogite sample (TM107) has SiO₂ of (47.02 wt. %), Fe₂O_{3T} (13.92 wt. %),
226 TiO₂(1.84 wt. %), MgO (7.34 wt. %), Na₂O (2.55 wt. %), CaO (7.94 wt. %), K₂O
227 (0.65 wt. %), and negligible P₂O₅. The eclogite is characterized by a slightly enriched
228 light-rare-earth element pattern (La/Yb = 2.68). It shares a typical composition with
229 that of enriched middle-ocean ridge basalt (E-MORB) (Sun and McDonough, 1989)
230 (Fig. 4a; Table 1). The garnet is relatively homogenous with Fe and Al, belonging to
231 the almandine end-member, and shows a decrease in Mn from the core to the rim
232 along a profile across the mineral (Fig. 4b). The compositions of minerals and bulk-
233 rock are presented in detail in Table 1 and Supplemental Table. The garnet-derived
234 P-T conditions constrain a prograde path with a maximum P-T condition of 2.2 GPa
235 and 560°C and a geothermal gradient of 7.7°C/km (Fig. 4c). Exhumation of the
236 eclogite resulted in the production of epidote and amphibole following peak
237 metamorphism. The modeling result agrees with the thin section observations,
238 indicating that rutile formed at the garnet rim during peak metamorphism. A total of

239 32 rutile grains (each with a 100 μm crystal size) was measured for U-Pb isotopes,
240 with 24 grains providing valid data (Table 2). The U concentration is modest (1.8–0.3
241 ppm), while the Th/U ratio varies between 0.01 and 0.33. The valid 24 analyses yield
242 a lower intercept age of 190 ± 11 Ma (1σ) with an MSWD of 1.9., as shown on the
243 Terra-Wasserburg diagram (Fig. 4d).

244

245 4. Discussion

246 4.1. Neo-Tethyan subduction initiation time

247 Most researchers agree that Neo-Tethyan subduction began at the southern
248 margin of Central Iran, but disagree on the timing of initiation between the Triassic-
249 Jurassic (Arvin et al., 2007; Ahadnejad et al., 2011; Chiu et al., 2013; Davoudian et
250 al., 2016; Zhang et al., 2018) and the late Cretaceous (Moghadam and Stern, 2015).
251 The widespread magmatism in the early Jurassic in Central Iran clearly shows arc
252 signatures of depleted Hf isotopes (Chiu et al., 2017; Zhang et al., 2018), which are
253 regarded as an upper constraint (earliest age) of subduction initiation. Some
254 researchers attribute a late Triassic Siah-Kuh granite (200 ± 30 Ma (2σ) Sm-Nd
255 isochron as the earliest evidence (Arvin et al., 2007). However, the updated LA-
256 ICPMS zircon U-Pb dating gave ages of 175 ± 1.8 Ma (2σ) from the Siah-Kuh granite
257 (Chiu et al., 2013), and now the earliest and most reliable arc magmatism in
258 southern Iran is a 187 ± 6 Ma (2σ) granodiorite (Ahadnejad et al., 2011) (Fig. 2).
259 Stern (2004) suggested that the age of the SSZ-type ophiolite could represent
260 subduction initiation. The earliest SSZ-type ophiolites in southern Central Iran along

261 the Turkish-Zagros suture formed 90 ± 10 Ma (Whattam and Stern, 2011;
262 Moghadam and Stern, 2015), which is significantly younger than the Jurassic
263 subduction arc magmatism (Zhang et al., 2018).

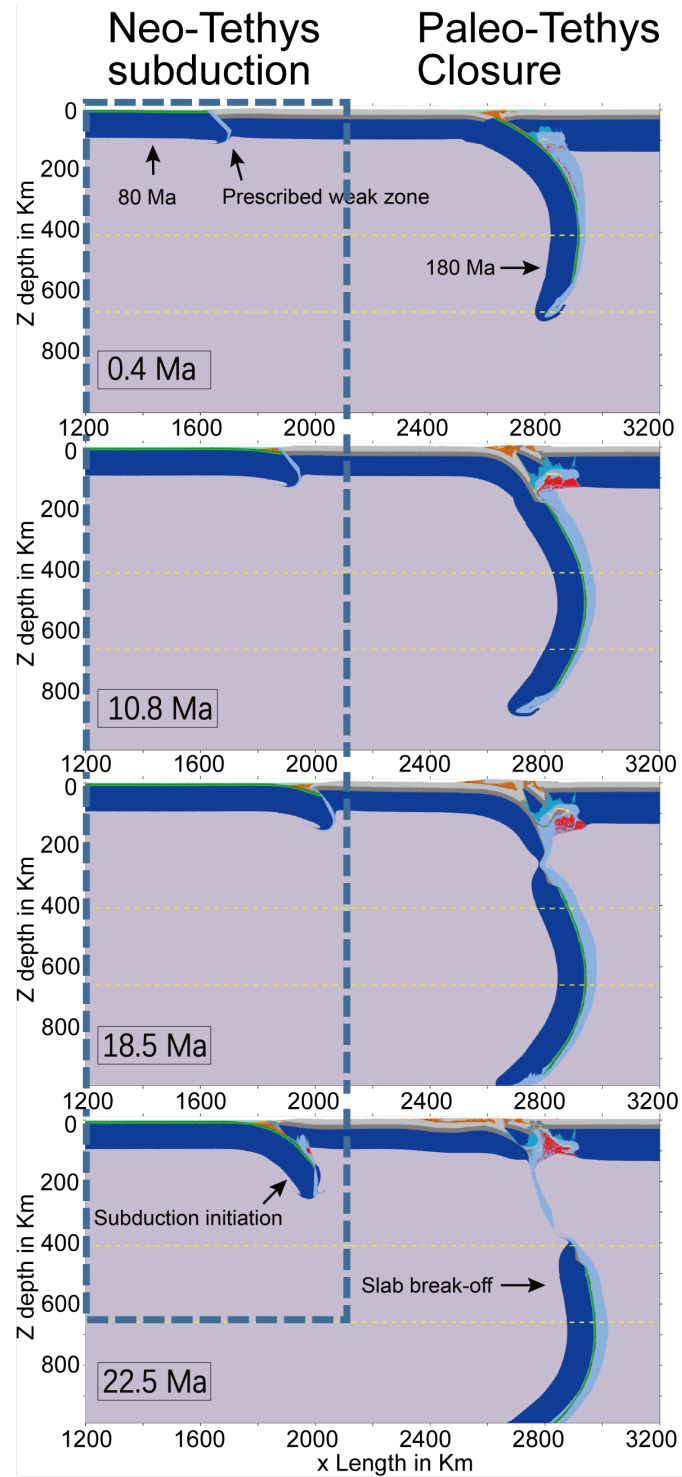
264 In contrast, the oldest HP rocks associated with subduction in the accretionary
265 complex may provide better evidence for subduction initiation. Using the phengite Ar-
266 Ar technique, the earliest eclogite was dated as being 184 ± 1 Ma (1σ) (Davoudian et
267 al., 2016). The sub-arc depth is known to be 100 kilometers, which corresponds to
268 the location of the majority of arc magma production (Syracuse and Abers, 2006).
269 HP metamorphism in a subduction zone mostly occurs at a fore-arc depth that is
270 shallower than the sub-arc depth (Agard et al., 2009). As a result, the earliest HP
271 metamorphic age in the subduction zone should be older than the earliest magmatic
272 arc rock formed following subduction initiation (only if these rocks have been
273 preserved and discovered). The eclogite contains E-MORB geochemistry that is
274 consistent with a previous report by Malek-Mahmoudi et al. (2017), indicating an
275 oceanic slab subduction environment (Fig. 4). The in-situ rutile U-Pb dating method
276 yielded an age of 190 ± 11 Ma (1σ) with an MSWD of 1.9. This new in-situ rutile age
277 is slightly older than the oldest arc magmatism (187 Ma) in Central Iran. The Mn
278 concentration of garnet from the eclogite is enriched in the core and is depleted in
279 the rim, indicating that the eclogite was under prograde metamorphism (Fig. 4d).

280 This study calculates that the eclogites experienced a geothermal gradient of 7° –
281 7.7° °C/km, which replicates the results from Davoudian et al. (2016). These
282 temperatures are within typical subduction zone geothermal gradients of 5 – 10° °C/km

283 (Wang et al., 2021). However, numerous geological and numerical investigations
284 revealed a hot subduction environment during subduction initiation that is
285 characterized by high-temperature rocks such as boninite and a metamorphic sole
286 (Stern, 2004; Esna-Ashari et al., 2016; Maunder et al., 2020; Coulthard Jr et al.,
287 2021). While the new rutile U-Pb age from the eclogite sample constrains the oldest
288 subduction-related timing in the Iranian Neo-Tethyan region to date, it represents the
289 closest time lagged after the subduction initiation with respect to previous studies
290 (Ahadnejad et al., 2011; Davoudian et al., 2016). Unlike the records in Iran, Early
291 Jurassic ophiolites and accretionary complexes are well documented in Turkey, to
292 the west of Iran, along the strike (Topuz et al., 2013; Okay et al., 2020). The geology
293 in Turkey would help the correlation of the Jurassic subduction zone along the
294 southern Eurasian margin, in southern Iran with the nearby region.

295 Nikolaeva et al. (2010) modeling experiments suggest that the transition from a
296 stable margin to subduction initiation at a passive margin is controlled by the ductile
297 strength of the lower continental crust, subcontinental lithospheric mantle, and the
298 density contrast with the suboceanic lithospheric mantle. The modeled transition
299 takes 1 Myr to ~45 Myr to initiate subduction. However, new numerical modeling
300 examined the time of subduction initiation at passive margins, and determined that
301 subduction could occur only in the presence of a weak zone at the passive margin
302 Zhong and Li (2020). If a horizontal convergence force (larger than 3.0×10^{12} N/m)
303 is exerted on the passive margin, the transition duration from passive to subduction
304 is between ~2 Myr to ~20 Myr, but for most cases are less than 10 Myr (Zhong and

305 Li, 2020). As previously estimated, the subduction plate at 700 km depth would exert
306 4.9×10^{13} N/m force on the trench plate (Wan et al., 2021). Previous modeling
307 shows that the net slab force to pull the trailing plate is 10% of the slab pull force
308 (Schellart, 2004), $\sim 4.9 \times 10^{12}$ N/m for the Iranian Tethys case. After initial collision,
309 and before slab breakoff, the net slab pull force together with the ridge push force
310 from Neo-Tethyan mid-ocean should match the numerical modeling requirements of
311 Zhong and Li (2020). The new rutile age of 190 ± 11 Ma (1σ) from the geological
312 observation is not conflict with the results from numerical tests in Zhong and Li
313 (2020)(Fig. 5). The earliest subduction initiation at a passive margin should occur
314 between 192 and 210 Ma.



315

316 **Figure 5. Convergent boundary force of 3.0×10^{12} N/m, with a prescribed weak**
 317 **zone at the passive margin model showing the subduction initiation taking**
 318 **22.5 Myr after collision. Dashed boxes mark the passive margin. After**
 319 **Zhong and Li (2020)**

320

321 4.2. Mechanism of Neo-Tethyan subduction initiation from the Eurasian 322 margin

323 The boundary between the Neo-Tethyan oceanic plate and Central Iran
324 continental crust is the location where the Neo-Tethyan subduction zone initiated.
325 This is because no earlier oceanic island arc (older than 100–120 Ma) has been
326 reported in the southern Central Iran (Moghadam and Stern, 2011; Moghadam and
327 Stern, 2015). Central Iran has a current size of approximately 1 million km².
328 Considering the shortening rate of Central Iran during the Arabian-Eurasian collision,
329 including the older Cimmerian orogeny, its original size must be larger than its
330 current size and could be comparable with the size of the Ontong Java oceanic
331 plateau of 1.5 million km². Niu et al. (2003) showed that a plume-modified oceanic
332 lithosphere is ~1% less dense than a normal oceanic lithosphere. According to new
333 numerical modeling studies, an oceanic plateau with a strong rheological and
334 depleted mantle root could assist the subduction zone by transferring from a plateau-
335 continent collision zone to a plateau-oceanic boundary (Yan et al., 2021). Central
336 Iran must be even lighter than an oceanic plateau because of the lighter continental
337 lithosphere and thicker and lighter sedimentary cover. Therefore, its resistance to
338 subduction during collision should be even more likely. To induce a new subduction
339 zone, it is necessary to provide a continuous convergent force to overcome the
340 lithospheric rigidity. The convergent force at the southern margin of Central Iran is
341 controlled by the interplay between Central Iran and Eurasia colliding. The northward
342 collision force is provided by the Paleo-Tethyan slab's northward subduction prior to

343 its separation from Central Iran and its lateral continents. According to van Hunen
344 and Allen (2011) numerical modeling experiments, the older the oceanic crust is, the
345 stronger it is and requires a longer period (over 20 Myr) to break-off. Because the
346 Paleo-Tethyan opening occurred earlier than the Devonian (Chu et al., 2021), the
347 late Triassic collision formed the subducting boundary between the Paleo-Tethyan
348 slab and Central Iran. Such a prolonged time span indicates the presence of a strong
349 oceanic lithosphere. As a result, the subducting Paleo-Tethyan slab may give at
350 least another 20 Myr of convergence following collision. The docking/amalgamation
351 and growth of mountains in northern Iran may have absorbed part of the horizontal
352 convergence. However, kilometer-scale uplift cannot absorb all of the convergence
353 from hundreds or even thousands of kilometers of continental collision. Following the
354 ultimate break-off of the Paleo-Tethyan slab, the low density continental crust in the
355 mantle will be exhumed to a shallow depth due to its buoyancy, providing an extra
356 force to supply the southern Central Iran margin with the convergent force required
357 to initiate subduction. Thus, following continental collision, several geological
358 processes may generate horizontal convergence stresses sufficient to initiate
359 subduction along pre-existing weak zones in the Gondwana lithosphere (Fig. 5d).

360 The newly constrained timing of collision at 228–209 Ma indicates that a
361 continuous convergent force can continue to 208–189 Ma before slab break-off (van
362 Hunen and Allen, 2011; Zhong and Li, 2020; Chu et al., 2021). This coincides with
363 our new predicted Neo-Tethyan subduction initiation time range of 210–192 Ma. This
364 study's limitation is that observation of geological events such as continental collision,

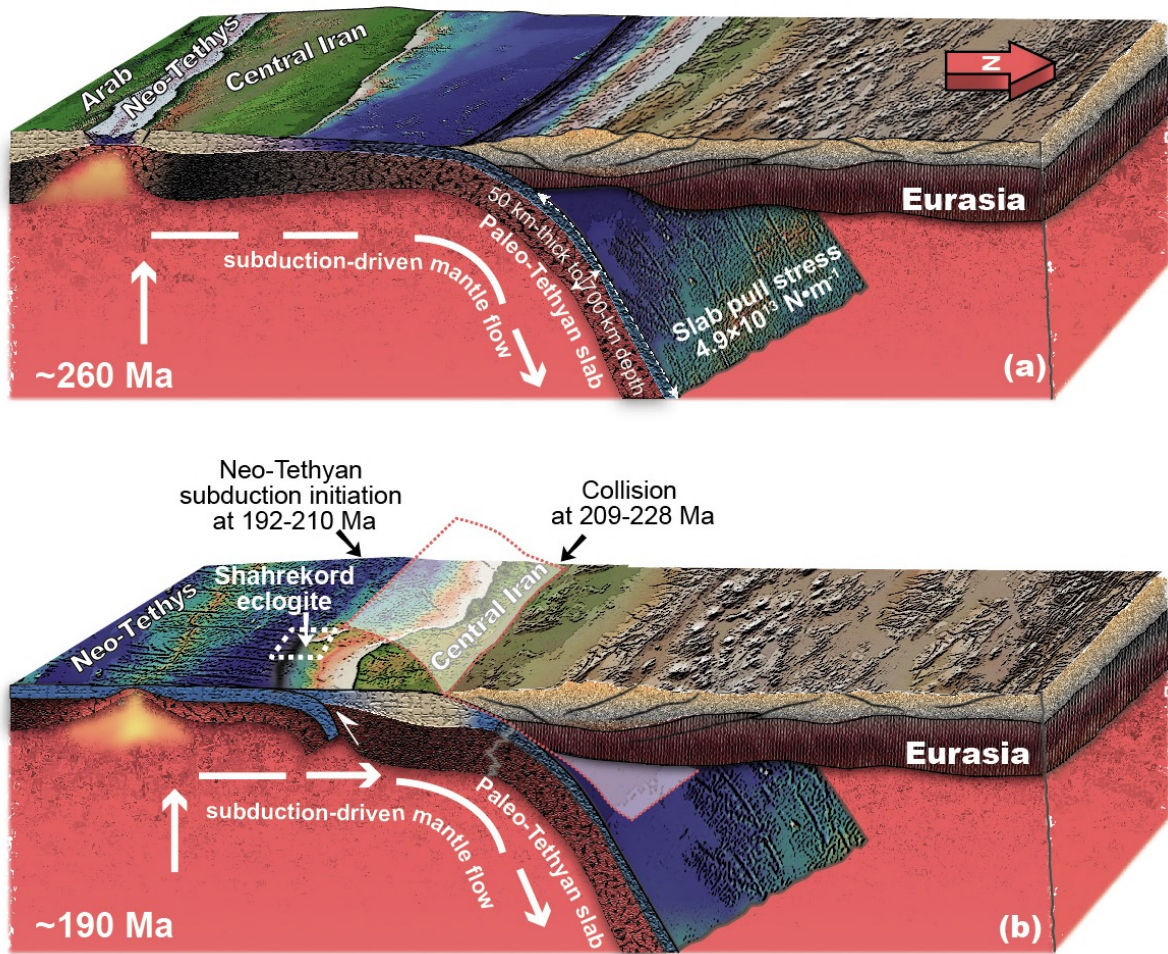
365 subduction initiation, and accompanying slab break-off, cannot be as precise as
366 numerical modeling, and geological events may be diachronous along strike.
367 However, the sequence between continental collision and subduction initiation
368 remains constant. According to updated information, the Iranian Neo-Tethys
369 subduction began between 210 and 192 Ma, which is younger than the final closure
370 of the Paleo-Tethys in northern Iran, which occurred between 228 and 209 Ma (Fig.
371 6a). Similar scenarios occurred in other Tethyan regions, such as in Bulgaria, Turkey,
372 Tibet, and southeast Asian regions (see Wan et al., 2019 and references therein),
373 which may have broad implications for subduction zone transfer in Tethyan collision
374 events.

375 The Neo-Tethyan region's continental collision-induced subduction initiation may
376 be distinct from the Pacific region, as there are numerous cases of subduction
377 polarity reversal in the south to west Pacific (Brown and Ryan, 2011). During the
378 Tethyan development, the new subduction in the Neo-Tethys and Indian Oceans
379 began along the Eurasian continental margin and moved the drifting Gondwanan
380 blocks towards the Eurasian continent because of northward oceanic subduction.
381 There may have been a unique feature during the creation of the southern Eurasian
382 passive margin. The rifting process created several faults along the continental
383 margin, which may serve as weak zones for future subduction. Central Iran was
384 located upon a mantle convection cell defined by the sinking of the Paleo-Tethyan
385 slab in the north and the upwelling of mantle in the Neo-Tethyan ridge in the south,
386 during the interval between the Neo-Tethys opening and the Paleo-Tethyan closing.

387 According to subduction-driven plate tectonics of Forsyth and Uyeda (1975), the
388 convection cell was driven by the downgoing Paleo-Tethyan oceanic slab and should
389 continue to function even after the Paleo-Tethyan oceanic slab split from Central Iran
390 (Conrad and Lithgow-Bertelloni, 2002). Taken together, the normal convergent force
391 ($3-5 \times 10^{12}$ N/m) at the abrupt continent-oceanic boundary via pre-existing faults and
392 a continuing northward mantle movement beneath the continent are likely the
393 reasons for the subduction to begin along the southern Eurasian margin following
394 continental collision (Fig. 6b).

395 Many researchers proposed that the whole-mantle convection that is bounded by
396 upwelling of mantle plumes beneath Gondwana and downwelling beneath Eurasia
397 may have played important roles for the Tethyan evolution (e.g. Becker and
398 Faccenna, 2011; Jolivet et al., 2016; Faccenna et al., 2021). In our studies, we
399 proposed that the subduction beneath Eurasia could cause continental rifting from
400 Gondwana (Wan et al., 2021), drive continental northward drifting and trigger
401 subduction initiation along the southern Eurasian margin. The major difference
402 between the whole-mantle convection model and the subduction-driven model is that
403 the upwelling of mantle plumes plays an active role in the long-lived single-directed
404 Tethyan evolution or it is only a **passive** feedback of the slab subduction towards
405 Eurasia (Chen et al., 2020). To gain deep insight into this issue demands more
406 whole-mantle scale studies and more geological cases in the earlier history than
407 Paleo-Tethys (Coltice et al., 2019; Robert et al., 2020; Wu et al., 2020).

408



409

410 **Figure 6. (a) Paleo-Tethyan subduction leads rifting to open Neo-Tethys in Iran,**

411 **revised from Wan et al. (2021), (b) Collision induced Neo-Tethyan subduction**

412 **initiation along the passive margin of central Iran.**

413 5. Conclusions

- 414 • At $190 \pm 11 \text{ Ma}$ (1σ) from rutile U-Pb dates, a prograde-E-MORB-like eclogite
- 415 along the Neo-Tethyan suture reached peak metamorphic condition of 2.2 GPa
- 416 and 560°C . This age represents the youngest (latest) age for subduction
- 417 initiation of Neo-Tethys.
- 418 • Based on regional geological events and numerical modeling results, the oldest
- 419 Neo-Tethyan subduction initiation date is 192–210 Ma, which is slightly younger

420 than the Paleo-Tethyan closure timing of 209–228 Ma, implying collision-induced
421 subduction initiation.

422 • During the rifting of Neo-Tethys, the southern margin of Central Iran inherited
423 pre-existing faults. At such a boundary, the collision-induced force, combined
424 with subduction-driving mantle flow, may aid in the initiation of northward
425 subduction.

426

427 Acknowledgement

428 We thank Dr. Elizabeth J. Catlos for the invitation for this contribution. We appreciate the
429 logistical help from colleagues at GSI during the fieldwork in Iran. We thank Dr. Wang, JM
430 and Chen, Y for the P-T reconstructions. Discussions with Lin, W., Wu, FY., and Xiao, WJ.
431 help to improve our interpretations. We thank R. Hansman for improving our writing.
432 Comments from three anonymous reviewers and Dr. Jamshid Hassanzadeh clarify our
433 original idea. This study was supported by the NSFC grants (91855207, 41888101).

434 References

- 435 Agard, P., J. Omrani, L. Jolivet, H. Whitechurch, B. Vrielynck, W. Spakman, P. Monie, B. Meyer, and
436 R. Wortel (2011), Zagros orogeny: a subduction-dominated process, *Geological Magazine*, 148(5-
437 6), 692-725, doi:10.1017/S001675681100046x.
- 438 Agard, P., P. Yamato, L. Jolivet, and E. Burov (2009), Exhumation of oceanic blueschists and
439 eclogites in subduction zones: Timing and mechanisms, *Earth-Sci. Rev.*, 92(1–2), 53-79,
440 doi:10.1016/j.earscirev.2008.11.002.
- 441 Ahadnejad, V., M.-V. Valizadeh, R. Deevsalar, and M. Rezaei-Kahkhaei (2011), Age and geotectonic
442 position of the Malayer granitoids: Implication for plutonism in the Sanandaj-Sirjan Zone, W Iran,
443 *Neues Jahrbuch für Geologie und Paläontologie-Abhandlungen*, 261(1), 61-75.

444 Ao, S. J., W. J. Xiao, M. K. Jafari, M. Talebian, L. Chen, B. Wan, W. Q. Ji, and Z. Y. Zhang (2016), U-
445 Pb zircon ages, field geology and geochemistry of the Kermanshah ophiolite (Iran): From
446 continental rifting at 79 Ma to oceanic core complex at ca. 36 Ma in the southern Neo-Tethys,
447 *Gondwana Research*, 31, 305-318, doi:10.1016/j.gr.2015.01.014.

448 Arvin, M., Y. Pan, S. Dargahi, A. Malekizadeh, and A. Babaei (2007), Petrochemistry of the Siah-Kuh
449 granitoid stock southwest of Kerman, Iran: Implications for initiation of Neotethys subduction,
450 *Journal of Asian Earth Sciences*, 30(3-4), 474-489.

451 Azizi, H., and R. J. Stern (2019), Jurassic igneous rocks of the central Sanandaj–Sirjan zone (Iran)
452 mark a propagating continental rift, not a magmatic arc, *Terra Nova*, 31(5), 415-423,
453 doi:10.1111/ter.12404.

454 Becker, T. W., and C. Faccenna (2011), Mantle conveyor beneath the Tethyan collisional belt, *Earth
455 and Planetary Science Letters*, 310(3-4), 453-461, doi:10.1016/j.epsl.2011.08.021.

456 Bergman, S. C., J. S. Eldrett, and D. Minisini (2021), Phanerozoic Large Igneous Province, Petroleum
457 System, and Source Rock Links, in *Large Igneous Provinces*, edited, pp. 191-228,
458 doi:10.1002/9781119507444.ch9.

459 Bonnet, G., P. Agard, H. Whitechurch, M. Fournier, S. Angiboust, B. Caron, and J. Omrani (2020),
460 Fossil seamount in southeast Zagros records intraoceanic arc to back-arc transition: New
461 constraints for the evolution of the Neotethys, *Gondwana Research*, 81, 423-444,
462 doi:10.1016/j.gr.2019.10.019.

463 Brown, D., and P. D. Ryan (2011), *Arc-continent collision*, 493 pp., Springer Science & Business
464 Media, Springer Heidelberg Dordrecht London New York.

465 Chen, L., X. Wang, X. Liang, B. Wan, and L. Liu (2020), Subduction tectonics vs. Plume tectonics—
466 Discussion on driving forces for plate motion, *Science China Earth Sciences*, 63(3), 315-328,
467 doi:10.1007/s11430-019-9538-2.

468 Cherniak, D. J. (2000), Pb diffusion in rutile, *Contributions to Mineralogy and Petrology*, 139(2), 198-
469 207, doi:10.1007/PL00007671.

470 Chiu, H.-Y., S.-L. Chung, M. H. Zarrinkoub, R. Melkonyan, K.-N. Pang, H.-Y. Lee, K.-L. Wang, S. S.
471 Mohammadi, and M. M. Khatib (2017), Zircon Hf isotopic constraints on magmatic and tectonic
472 evolution in Iran: Implications for crustal growth in the Tethyan orogenic belt, *Journal of Asian
473 Earth Sciences*, 145, 652-669, doi:10.1016/j.jseaes.2017.06.011.

474 Chiu, H.-Y., S.-L. Chung, M. H. Zarrinkoub, S. S. Mohammadi, M. M. Khatib, and Y. Iizuka (2013),
475 Zircon U–Pb age constraints from Iran on the magmatic evolution related to Neotethyan
476 subduction and Zagros orogeny, *Lithos*, 162–163, 70-87, doi:10.1016/j.lithos.2013.01.006.

477 Chu, Y., B. Wan, M. B. Allen, L. Chen, W. Lin, M. Talebian, and G. Xin (2021), Detrital zircon age
478 constraints on the evolution of Paleo-Tethys in NE Iran: implications for subduction and collision
479 tectonics, *Tectonics*, 40, e2020TC006680, doi:10.1029/2020TC006680.

480 Coltice, N., L. Husson, C. Faccenna, and M. Arnould (2019), What drives tectonic plates?, *Science*
481 *Advances*, 5(10), eaax4295, doi:10.1126/sciadv.aax4295.

482 Conrad, C. P., and C. Lithgow-Bertelloni (2002), How mantle slabs drive plate tectonics, *Science*,
483 298(5591), 207-209, doi:10.1126/science.1074161.

484 Coulthard Jr, D. A., M. K. Reagan, K. Shimizu, I. N. Bindeman, M. Brounce, R. R. Almeev, J. Ryan, T.
485 Chapman, J. Shervais, and J. A. Pearce (2021), Magma Source Evolution Following Subduction
486 Initiation: Evidence From the Element Concentrations, Stable Isotope Ratios, and Water Contents
487 of Volcanic Glasses From the Bonin Forearc (IODP Expedition 352), *Geochemistry, Geophysics,*
488 *Geosystems*, 22(1), doi:10.1029/2020gc009054.

489 Davoudian, A. R., J. Genser, F. Neubauer, and N. Shabanian (2016), ⁴⁰Ar/³⁹Ar mineral ages of
490 eclogites from North Shahrekord in the Sanandaj–Sirjan Zone, Iran: Implications for the tectonic
491 evolution of Zagros orogen, *Gondwana Research*, 37, 216-240, doi:10.1016/j.gr.2016.05.013.

492 DeMets, C., R. G. Gordon, and D. F. Argus (2010), Geologically current plate motions, *Geophysical*
493 *Journal International*, 181(1), 1-80, doi:10.1111/j.1365-246X.2009.04491.x.

494 Emami, N., and M. Khalili (2008), Mineralogical and geochemical constraints of Jurassic fossil
495 hydrothermal alteration associated with an calc-alkaline volcano-sedimentary complex in
496 Sanandaj-Sirjan Zone, Southwest of Iran, *Journal of Applied Sciences*, 8(9), 1600-1611.

497 Esna-Ashari, A., M. Tiepolo, and J. Hassanzadeh (2016), On the occurrence and implications of
498 Jurassic primary continental boninite-like melts in the Zagros orogen, *Lithos*, 258-259, 37-57,
499 doi:10.1016/j.lithos.2016.04.017.

500 Faccenna, C., T. W. Becker, A. F. Holt, and J. P. Brun (2021), Mountain building, mantle convection,
501 and supercontinents: revisited, *Earth and Planetary Science Letters*, 564,
502 doi:10.1016/j.epsl.2021.116905.

503 Forsyth, D., and S. Uyeda (1975), On the relative importance of the driving forces of plate motion,
504 *Geophysical Journal International*, 43(1), 163-200.

505 Fürsich, F. T., M. Wilmsen, K. Seyed-Emami, M. R. Majidifard, M.-F. Brunet, M. Wilmsen, and J. W.
506 Granath (2009), Lithostratigraphy of the Upper Triassic–Middle Jurassic Shemshak Group of
507 Northern Iran, in *South Caspian to Central Iran Basins*, edited, pp. 129-160, Geological Society of
508 London, doi:10.1144/sp312.6.

509 Gerya, T. V., R. J. Stern, M. Baes, S. V. Sobolev, and S. A. Whattam (2015), Plate tectonics on the
510 Earth triggered by plume-induced subduction initiation, *Nature*, 527(7577), 221-225,
511 doi:10.1038/nature15752.

512 Guilmette, C., M. A. Smit, D. J. J. van Hinsbergen, D. Gürer, F. Corfu, B. Charette, M. Maffione, O.
513 Rabeau, and D. Savard (2018), Forced subduction initiation recorded in the sole and crust of the
514 Semail Ophiolite of Oman, *Nature Geoscience*, 11(9), 688-695, doi:10.1038/s41561-018-0209-2.

515 Hall, R. (2017), Southeast Asia: new views of the geology of the Malay archipelago, *Annual Review of*
516 *Earth and Planetary Sciences*, 45(1), 331-358, doi:10.1146/annurev-earth-063016-020633.

517 Hassanzadeh, J., and B. P. Wernicke (2016), The Neotethyan Sanandaj-Sirjan zone of Iran as an
518 archetype for passive margin-arc transitions, *Tectonics*, 35(3), 586-621,
519 doi:10.1002/2015tc003926.

520 Jamali Ashtiani, R., J. Hassanzadeh, A. K. Schmitt, M. Sudo, M. Timmerman, C. Günter, and E. Sobel
521 (2020), Geochronology and geochemistry of subducted Cadomian continental basement in central
522 Iran: Decompressional anatexis along the Jurassic Neotethys margin, *Gondwana Research*, 82,
523 354-366, doi:10.1016/j.gr.2020.01.005.

524 Jolivet, L., C. Faccenna, P. Agard, D. Frizon de Lamotte, A. Menant, P. Sternai, F. Guillocheau, and
525 A. Polat (2016), Neo-Tethys geodynamics and mantle convection: from extension to compression
526 in Africa and a conceptual model for obduction, *Canadian Journal of Earth Sciences*, 53(11), 1190-
527 1204, doi:10.1139/cjes-2015-0118.

528 Koop, W., R. Stoneley, M. Ridd, R. Murphy, M. Osmaston, and M. Kholief (1982), Subsidence history
529 of the middle east Zagros Basin, Permian to recent, *Philosophical Transactions of The Royal*
530 *Society A: Mathematical, Physical and Engineering Sciences*, 305, 149-167,
531 doi:10.1098/rsta.1982.0031.

532 Lawver, L. A., I. W. Dalziel, I. O. Norton, L. Gahagan, and J. Davis (2015), The PLATES 2014 Atlas of
533 Plate Reconstructions (550 Ma to Present Day), PLATES Progress Report No. 374-0215,
534 *University of Texas Institute for Geophysics Technical Reports*, 220.

535 Leng, W., and M. Gurnis (2015), Subduction initiation at relic arcs, *Geophysical Research Letters*,
536 42(17), 7014-7021.

537 Leven, E. J., and M. N. Gorgij (2011), Fusulinids and stratigraphy of the Carboniferous and Permian
538 in Iran, *Stratigr. Geol. Correl.*, 19(7), 687-776, doi:10.1134/s0869593811070021.

539 Malek-Mahmoudi, F., A. Reza Davoudian, N. Shabanian, H. Azizi, Y. Asahara, F. Neubauer, and Y.
540 Dong (2017), Geochemistry of metabasites from the North Shahrekord metamorphic complex,

541 Sanandaj-Sirjan Zone: Geodynamic implications for the Pan-African basement in Iran,
542 *Precambrian Research*, 293, 56-72, doi:10.1016/j.precamres.2017.03.003.

543 Maunder, B., J. Prytulak, S. Goes, and M. Reagan (2020), Rapid subduction initiation and magmatism
544 in the Western Pacific driven by internal vertical forces, *Nature communications*, 11(1), 1874,
545 doi:10.1038/s41467-020-15737-4.

546 McQuarrie, N., and D. J. J. van Hinsbergen (2013), Retrodeforming the Arabia-Eurasia collision zone:
547 Age of collision versus magnitude of continental subduction, *Geology*, 41(3), 315-318,
548 doi:10.1130/G33591.1.

549 Merdith, A. S., S. E. Williams, S. Brune, A. S. Collins, and R. D. Müller (2019), Rift and plate boundary
550 evolution across two supercontinent cycles, *Global and Planetary Change*, 173, 1-14,
551 doi:10.1016/j.gloplacha.2018.11.006.

552 Moghadam, H. S., Q.-L. Li, W. L. Griffin, R. J. Stern, J. F. Santos, M. N. Ducea, C. J. Ottley, O. Karsli,
553 F. Sepidbar, and S. Y. O'Reilly (2022), Temporal changes in subduction- to collision-related
554 magmatism in the Neotethyan orogen: The Southeast Iran example, *Earth-Sci. Rev.*, 226, 103930,
555 doi:10.1016/j.earscirev.2022.103930.

556 Moghadam, H. S., and R. J. Stern (2011), Geodynamic evolution of Upper Cretaceous Zagros
557 ophiolites: formation of oceanic lithosphere above a nascent subduction zone, *Geological*
558 *Magazine*, 148(5-6), 762-801.

559 Moghadam, H. S., and R. J. Stern (2015), Ophiolites of Iran: Keys to understanding the tectonic
560 evolution of SW Asia: (II) Mesozoic ophiolites, *Journal of Asian Earth Sciences*, 100(0), 31-59,
561 doi:10.1016/j.jseaes.2014.12.016.

562 Natal'in, B. A., and A. M. C. Şengör (2005), Late Palaeozoic to Triassic evolution of the Turan and
563 Scythian platforms: The pre-history of the Palaeo-Tethyan closure, *Tectonophysics*, 404(3), 175-
564 202, doi:10.1016/j.tecto.2005.04.011.

565 Nikolaeva, K., T. V. Gerya, and F. O. Marques (2010), Subduction initiation at passive margins:
566 Numerical modeling, *Journal of Geophysical Research*, 115(B3), 10.1029/2009JB006549,
567 doi:10.1029/2009jb006549.

568 Niu, Y., M. J. O'Hara, and J. A. Pearce (2003), Initiation of subduction zones as a consequence of
569 lateral compositional buoyancy contrast within the lithosphere: a petrological perspective, *Journal*
570 *of Petrology*, 44(5), 851-866, doi:10.1093/petrology/44.5.851.

571 Okay, A. I., G. Sunal, S. Sherlock, A. R. C. Kylander - Clark, and E. Özcan (2020), İzmir - Ankara
572 Suture as a Triassic to Cretaceous Plate Boundary—Data From Central Anatolia, *Tectonics*, 39(5),
573 doi:10.1029/2019tc005849.

574 Omrani, J., P. Agard, H. Whitechurch, M. Benoit, G. Prouteau, and L. Jolivet (2008), Arc-magmatism
575 and subduction history beneath the Zagros Mountains, Iran: A new report of adakites and
576 geodynamic consequences, *Lithos*, 106(3–4), 380-398, doi:10.1016/j.lithos.2008.09.008.

577 Robert, B., M. Domeier, and J. Jakob (2020), Iapetan Oceans: An analog of Tethys?, *Geology*, 48(9),
578 929-933, doi:10.1130/g47513.1.

579 Schellart, W. (2004), Quantifying the net slab pull force as a driving mechanism for plate tectonics,
580 *Geophysical Research Letters*, 31(7), doi:10.1029/2004gl019528.

581 Scotese, C. R., H. Song, B. J. W. Mills, and D. G. van der Meer (2021), Phanerozoic
582 paleotemperatures: The earth's changing climate during the last 540 million years, *Earth-Sci. Rev.*,
583 215, doi:10.1016/j.earscirev.2021.103503.

584 Stampfli, G. M., C. Hochard, C. V  rard, C. Wilhem, and J. vonRaumer (2013), The formation of
585 Pangea, *Tectonophysics*, 593, 1-19, doi:10.1016/j.tecto.2013.02.037.

586 Stern, R. J. (2004), Subduction initiation: spontaneous and induced, *Earth and Planetary Science*
587 *Letters*, 226(3-4), 275-292, doi:10.1016/j.epsl.2004.08.007.

588 Stern, R. J., and T. Gerya (2018), Subduction initiation in nature and models: A review,
589 *Tectonophysics*, 746, 173-198, doi:10.1016/j.tecto.2017.10.014.

590 Stern, R. J., H. S. Moghadam, M. Pirouz, and W. Mooney (2021), The Geodynamic Evolution of Iran,
591 *Annual Review of Earth and Planetary Sciences*, 49(1), 9-36, doi:10.1146/annurev-earth-071620-
592 052109.

593 Sun, S. S., and W. F. McDonough (1989), Chemical and isotopic systematics of ocean basins:
594 implications for mantle composition and processes, *Geological Society of London, Special*
595 *Publications*, 42, 313-345.

596 Syracuse, E. M., and G. A. Abers (2006), Global compilation of variations in slab depth beneath arc
597 volcanoes and implications, *Geochemistry, Geophysics, Geosystems*, 7(5),
598 doi:10.1029/2005GC001045.

599 Topuz, G. I., G. G   mengil, Y. Rolland,   . F.    elik, T. Zack, and A. K. Schmitt (2013), Jurassic
600 accretionary complex and ophiolite from northeast Turkey: No evidence for the Cimmerian
601 continental ribbon, *Geology*, 41(2), 255-258, doi:10.1130/g33577.1.

602 Torsvik, T. H., and L. R. M. Cocks (2017), *Earth history and palaeogeography*, 317 pp., Cambridge
603 University Press, United Kingdom, doi:10.1017/9781316225523.

604 van Hinsbergen, D. J. J., et al. (2021), A record of plume-induced plate rotation triggering subduction
605 initiation, *Nature Geoscience*, 14(8), 626-630, doi:10.1038/s41561-021-00780-7.

606 van Hunen, J., and M. B. Allen (2011), Continental collision and slab break-off: A comparison of 3-D
607 numerical models with observations, *Earth and Planetary Science Letters*, 302(1), 27-37.

608 Verdel, C., B. P. Wernicke, J. Hassanzadeh, and B. Guest (2011), A Paleogene extensional arc flare-
609 up in Iran, *Tectonics*, 30(3), doi:10.1029/2010tc002809.

610 Wakabayashi, J. (2011), Mélanges of the Franciscan Complex, California: Diverse structural settings,
611 evidence for sedimentary mixing, and their connection to subduction processes, *Geological society
612 of America bulletin Special Papers*, 480, 117-141, doi:10.1130/2011.2480(05).

613 Wan, B., Y. Chu, L. Chen, X. Liang, Z. Zhang, S. Ao, and M. Talebian (2021), Paleo-Tethys
614 subduction induced slab-drag opening the Neo-Tethys: Evidence from an Iranian segment of
615 Gondwana, *Earth-Sci. Rev.*, 103788, doi:10.1016/j.earscirev.2021.103788.

616 Wan, B., F. Wu, L. Chen, L. Zhao, X. Liang, W. Xiao, and R. Zhu (2019), Cyclical one-way continental
617 rupture-drift in the Tethyan evolution: Subduction-driven plate tectonics, *Science China Earth
618 Sciences*, 62, 2005-2016, doi:10.1007/s11430-019-9393-4.

619 Wang, J.-M., P. Lanari, F.-Y. Wu, J.-J. Zhang, G. P. Khanal, and L. Yang (2021), First evidence of
620 eclogites overprinted by ultrahigh temperature metamorphism in Everest East, Himalaya:
621 Implications for collisional tectonics on early Earth, *Earth and Planetary Science Letters*, 558,
622 doi:10.1016/j.epsl.2021.116760.

623 Whattam, S. A., and R. J. Stern (2011), The 'subduction initiation rule': a key for linking ophiolites,
624 intra-oceanic forearcs, and subduction initiation, *Contributions to Mineralogy and Petrology*,
625 162(5), 1031-1045, doi:10.1007/s00410-011-0638-z.

626 Whittaker, J. M., S. E. Williams, and R. D. Müller (2013), Revised tectonic evolution of the Eastern
627 Indian Ocean, *Geochemistry, Geophysics, Geosystems*, 14(6), 1891-1909,
628 doi:10.1002/ggge.20120.

629 Williams, S. E., J. M. Whittaker, J. A. Halpin, and R. D. Müller (2019), Australian-Antarctic breakup
630 and seafloor spreading: Balancing geological and geophysical constraints, *Earth-Sci. Rev.*, 188,
631 41-58, doi:10.1016/j.earscirev.2018.10.011.

632 Wu, F. Y., B. Wan, L. Zhao, W. J. Xiao, and R. X. Zhu (2020), Tethyan geodynamics, *Acta
633 Petrologica Sinica*, 36(6), 1627-1674 (in Chinese with English abstract), doi:10.18654/1000-
634 0569/2020.06.01.

635 Yan, Z., L. Chen, X. Xiong, B. Wan, and H. Xu (2021), Oceanic plateau and subduction zone jump:
636 two - dimensional thermo - mechanical modeling, *Journal of Geophysical Research: Solid Earth*,
637 126(7), doi:10.1029/2021jb021855.

638 Zanchetta, S., F. Berra, A. Zanchi, M. Bergomi, M. Caridroit, A. Nicora, and G. Heidarzadeh (2013),
639 The record of the Late Palaeozoic active margin of the Palaeotethys in NE Iran: Constraints on the
640 Cimmerian orogeny, *Gondwana Research*, 24(3), 1237-1266, doi:10.1016/j.gr.2013.02.013.

641 Zhang, Z., et al. (2018), Geochemistry, zircon U-Pb and Hf isotope for granitoids, NW Sanandaj-Sirjan
642 zone, Iran: Implications for Mesozoic-Cenozoic episodic magmatism during Neo-Tethyan
643 lithospheric subduction, *Gondwana Research*, 62, 227-245, doi:10.1016/j.gr.2018.04.002.

644 Zhang, Z., W. Xiao, M. R. Majidifard, R. Zhu, B. Wan, S. Ao, L. Chen, M. Rezaeian, and R. Esmaili
645 (2017), Detrital zircon provenance analysis in the Zagros Orogen, SW Iran: implications for the
646 amalgamation history of the Neo-Tethys, *International Journal of Earth Sciences*, 106(4), 1223-
647 1238, doi:10.1007/s00531-016-1314-3.

648 Zhong, X., and Z.-H. Li (2020), Subduction initiation during collision-induced subduction transference:
649 numerical modeling and implications for the Tethyan evolution, *Journal of Geophysical Research:*
650 *Solid Earth*, 125(2), e2019JB019288, doi:10.1029/2019jb019288.

651 Zhong, X., and Z.-H. Li (2022), Wedge-Shaped Southern Indian Continental Margin Without Proper
652 Weakness Hinders Subduction Initiation, *Geochemistry, Geophysics, Geosystems*, 23(2),
653 e2021GC009998, doi:10.1029/2021GC009998.

654 Zhou, X., Z. H. Li, T. V. Gerya, and R. J. Stern (2020), Lateral propagation-induced subduction
655 initiation at passive continental margins controlled by preexisting lithospheric weakness, *Sci Adv*,
656 6(10), eaaz1048, doi:10.1126/sciadv.aaz1048.

657